Disordered magnetism in the homologue series $YBaCo_{4-x}Zn_xO_7$ (x = 0, 1, 2, 3)

2004 J. Phys.: Condens. Matter 16 9209

(http://iopscience.iop.org/0953-8984/16/50/012)

INSTITUTE OF PHYSICS PUBLISHING JOURNAL OF PHYSICS: CONDENSED MATTER

J. Phys.: Condens. Matter **16** (2004) 9209–9225 PII: S0953-8984(04)86950-9

Disordered magnetism in the homologue series $YBaCo_{4-x}Zn_xO_7$ ($x = 0, 1, 2, 3$)

Martin Valldor

Institut für Anorganische und Analytische Chemie, Universität Münster, Corrensstrasse 36, D-48149 Münster, Germany

E-mail: mvalldor@uni-muenster.de

Received 21 September 2004
Published 3 December 2004
Online at stacks.iop.org/JPhysCM/16/9209
doi:10.1088/0953-8984/16/50/012

Abstract

The magnetic properties of four compounds in the series $YBaCo_{4-x}Zn_xO_7$ ($x = 0, 1, 2, 3$) were investigated. For all compositions magnetic transitions were observed (T_f) over the temperature range 66–3 K observed with ac susceptibility and dc magnetometry. Futhermore, all ac measurements proved to be frequency-dependent: T_f increases with an increase in frequency. The real part of the magnetic susceptibility (χ') was, in all four cases, accompanied by an energy loss in the magnetic coupling, indicated as contributions to the imaginary part (χ''). The maximum χ'' appeared just below the maximum χ'. Using the Arrhenius law, the Vogel–Fulcher law and the power law, it was possible to conclude that the compounds should be defined as spin-glass-like materials. The dc magnetizations clearly show differences between field-cooled and zero-field-cooled measurements. None of the compounds exhibited any metamagnetic property and, using a new data analysis method, a possible saturation field could be calculated for $YBaCo_4O_7$. Relaxation measurements on $YBaCo_3ZnO_7$ indicate that the system has no ageing effects. The magnetic properties can be described as having two connected magnetic substructures represented as dimensionalities: axial (1D) and in-plane (2D). This was concluded by comparing the magnetic properties with structural details.

1. Introduction

Disordered magnetic materials have been known for a relatively long time. However, those systems also containing a perfect crystal structure can easily be counted. The most studied metal-oxide compounds, with disordered magnetic structures, are the pyroclores [1–5], the spinels [6–8] and a few of the underdoped superconductors [9, 10]. A new type of structure containing magnetic disorder was recently discovered: the defect wurtzite Co–O net in $YBaCo_4O_7$ [11]. This compound was studied further in a later report and exhibited chemical flexibility [12]. Many new stoichiometries gave rise to a large number of questions concerning

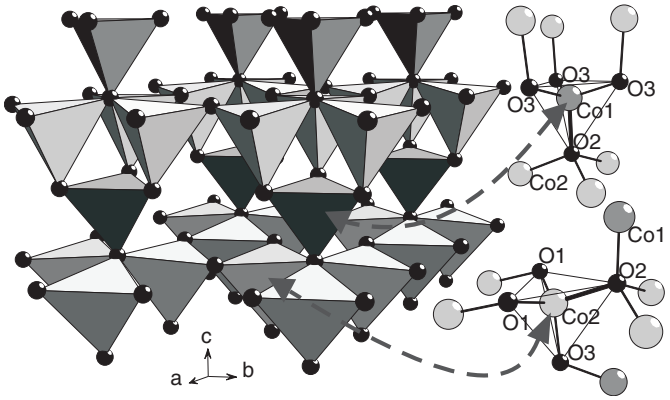

Figure 1. The Co–O net displayed as polyhedra (left) and ball-and-stick models (right). Arrows show the common points in the two presentation types. Oxygen is presented with black balls, Co1 with dark grey balls and polyhedra, while Co2 are the light grey balls and polyhedra.

the magnetic properties. The nature of the first compound, $YBaCo_4O_7$ [11], was not fully understood, even though there were many indications of a weak magnetic property, similar to the case of spin-glass materials. This is a follow-up paper focusing on the Y–Ba–Co–Zn–O system.

2. Description of the structure

The structure is thoroughly described in several papers [11–14] and all members in the homologue series $YBaCo_{4-x}Zn_xO_7$ ($x = 0$–3) are of this structure type. To be able to discuss some of the results presented in this paper, the substructure, containing the magnetic ions, is briefly described here. All Co and Zn atoms are tetrahedrally coordinated and represented in the structure with two crystallographic positions (Co1 and Co2 in figure 1), one of which is two-fold in the unit cell (Co1-2*a*) and the other six-fold (Co2-6*c*). The tetrahedra build up a net similar to the wurtzite structure that can be found for CoO [15]. However, in the (Co,Zn)O net, Ba and Y replace parts of the Co–O net. Structural analyses have shown that the tetrahedra themselves are asymmetric with metal–oxygen–metal angles and distances spanning a wide range [12]. Using simple calculations, it is possible to predict that one quarter of the tetrahedra must contain +3 ions and the rest +2 ions. Of Co and Zn, only Co can change its oxidation state between +2 and +3, resulting in the stoichiometry formula: $YBaCo^{3+}Co^{2+}_{3-x}Zn^{2+}_xO_7$ ($x = 0, 1, 2, 3$). The Co1 site was found to be generally smaller than the Co2 site [12], suggesting that the smaller Co1 site should contain relatively more Co^{3+} than the Co1 site. The oxygen stoichiometry is very close to 7 per unit formula, since any other situation would result in the unlikely plane–trigonal coordination of Co or Zn, since all oxygen positions are part of the tetrahedral net.

3. Experimental setup

The preparation and physical properties, such as structure and exact composition, have previously been published in [11, 12]. From these papers, the raw data have been taken for correlating the structure with the changing magnetic properties.

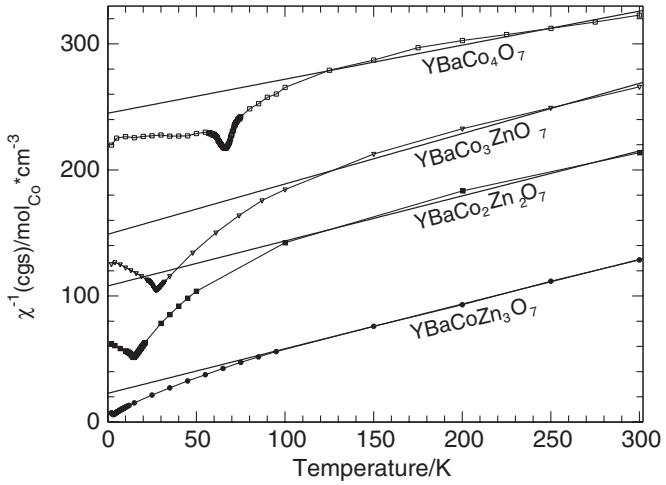

Figure 2. Reciprocal magnetic susceptibility, measured at 125 Hz and with an ac field of 10 Oe, plotted versus temperature.

Magnetization measurements over the range 2–300 K were performed with a SQUID MPMS from Quantum Design. Fields of up to 1 T were used during field cooling and 0.1 T was subsequently used during measurements.

Frequency-dependent magnetic susceptibility, field-dependent magnetization and field-cooled (FC), zero-field-cooled (ZFC) magnetic and thermoremanent magnetic relaxation measurements were performed in a PPMS from Quantum Design over the temperature range 2–300 K and fields from 0 to 8 T. For ac magnetic susceptibility, frequencies over the range 11–9975 Hz of a 10 Oe (1 mT) field were used. A field of 0.1 T was used during the freezing process for the magnetic relaxation measurements.

4. Results

4.1. Ac susceptibility

4.1.1. Curie–Weiss, Bohr magnetons. With the method of least squares, a fit to the $\chi^{-1}(T)$ was refined for all four compounds in the temperature region 100–300 K to extract the Weiss constant (θ_W). The linear fits are shown in figure 2 and all reach into the negative range $-907(50)$, $-373(50)$, $-303(30)$ and $-64(10)$ K for $x = 0$–3, respectively. The standard deviations are estimated and set high due to the small number of data points in the high-temperature region. Thus, the 'paramagnetic' region is influenced by temporary anti-ferromagnetic interactions in all four compounds. With higher Co content, the deviation from spin-only paramagnetism increases, i.e., the anti-parallel interactions become stronger.

Also, the magnetic transition, seen for all four compositions, has an upturn in the $\chi^{-1}(T)$ curve, which is commonly interpreted as an anti-ferromagnetic transition. The magnetic freezing temperature (T_f) changes with Co content: 66(1), 27(1), 15(1) and 3(1) K for $x = 0$–3, respectively.

If the magnetic interactions exhibit XY anisotropy, they can be evaluated [16] by applying the postulation of Kosterlitz and Thouless [17]. Using the Weiss constant for the different compounds, a theoretical value for the critical temperature, called T_{KT}, can be calculated by assuming a dimensionality of the magnetic coupling. In one extreme case (2D), T_{KT} should be

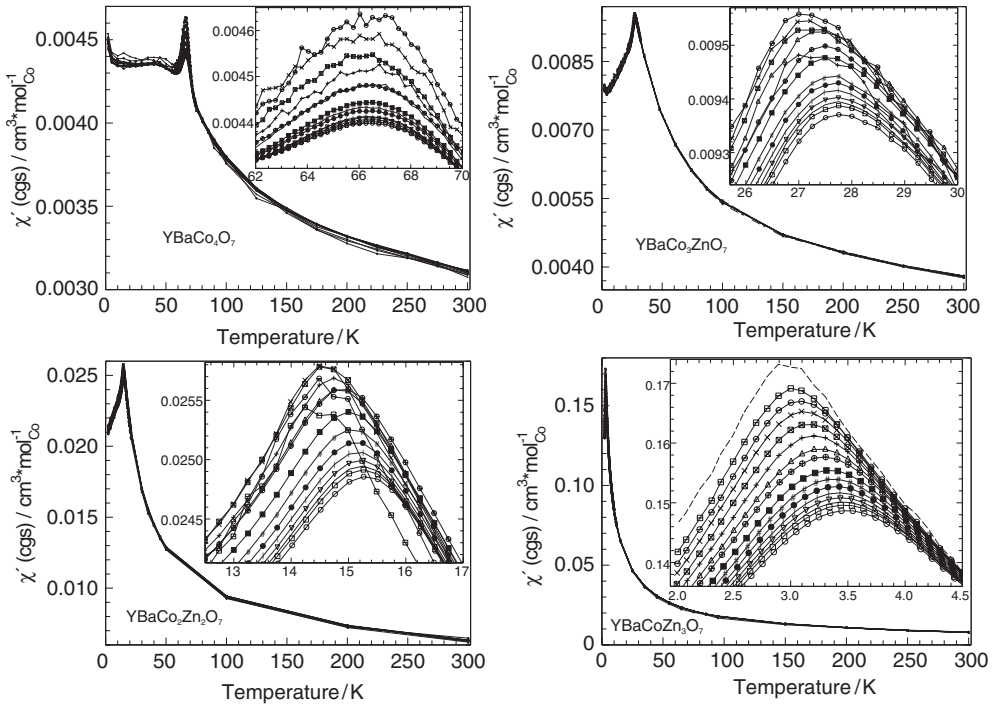

Figure 3. The magnetic susceptibility (real part $-\chi'$), using an ac field of 10 Oe, plotted versus temperature. The different compounds are indicated in the graphs and the inset is a magnification of the transition range. The measuring frequencies (in Hz) are: 11 (- - - -), 34 (⊟), 75 (⊖), 125 (×), 225 (⊠), 425 (×), 825 (△), 1225 (⊕), 2125 (■), 3025 (#), 4025 (●), 5025 (|), 6025 (▽), 7025 (no marker), 8025 (□) and 9975 (○).

$\theta_W/48$, where the divider originates from the Kosterlitz–Thouless formula. As a comparison, T_{KT} (2D) is calculated for the four compounds giving: −19(1), −7.8(1), −6.3(6) and −1.3(2) K for $x = 0$–3, respectively. This means that the compounds in this paper cannot be presented with a 2D model, since $T_f > T_{KT}$, or that the method does not work for this system.

Applying the Curie–Weiss law to the magnetic susceptibility data between 100 and 300 K, it was possible to calculate an average magnetic moment for Co: 5.44, 4.48, 4.74 and 4.76 μ_B for $x = 0$–3, respectively. Comparison with the literature (Co^{3+}: $\mu_{eff} = 4.9, \mu_{exp} = 4.3\mu_B$; Co^{2+}: $\mu_{eff} = 3.87, \mu_{exp} = 4.3\mu_B$ to $5.2\mu_B$ [18]) shows that the agreement between the literature and the experimentally obtained values is good, although there are only a few data points in that range.

In previous studies [11], the magnetic moment of Co was incorrectly calculated for $YBaCo_4O_7$, however the results presented herein are correctly calculated.

4.1.2. Ac suspectibility—real part. The real part of the magnetic susceptibility (χ') for the four different homologues is displayed in figure 3. All curves have paramagnetic type behaviour down to the transition, where the anti-ferromagnetic transition can be seen. Below the transition, the temperature dependence of χ' varies with every compound. For the $x = 3$ compound, there is only a linear decrease of susceptibility with a decrease in temperature down to 2 K. The next compound ($x = 2$) has, at first, a steep decrease in χ', but at ∼5 K below the transition the gradient becomes less pronounced. Also, in the next compound ($x = 1$), there is

a small change in the χ' gradient at ~20 K and an additional increase in susceptibility appears at ~5 K. The compound with only Co at the tetrahedral sites ($x = 0$) has a similar change in χ' 5–10 K below the first transition, however the curve turns almost flat and stays flat down to 5 K, where a similar increase in χ' as in the $x = 1$ compound can be seen.

When examining the insets to figure 3, it is also possible to conclude that all four compounds exhibit frequency-dependent T_f values; with higher ac frequency, an increase in T_f values can be observed. Therefore, it is assumed that the compounds have spin-glass or super-paramagnetic properties and will be treated accordingly in the discussion below. As a first comparison, the change in Co concentration (C) should change T_f, according to the relation $\Delta T_f/\Delta \log \omega \propto C$ [19]. This is calculated for a ~25-fold (225–6025 Hz) change of the ac frequency, giving the values 0.181, 0.281, 0.392 and 0.195 K $(\log \text{Hz})^{-1}$ for $x = 0$–3, respectively. The nonlinearity is obvious. This was also reported by Mulder *et al* [20] and they presented the formula $\Delta T_f/(T_f \times \Delta \log \omega)$, which in their case gave the same value independent of the percentage of magnetic ions in the non-magnetic matrix. For the presented compounds, this formula gives the values 0.0027, 0.010, 0.027 and 0.059 for $x = 0$–3, respectively; obviously, these values cannot be assumed equal. However, putting these values side by side with those gathered by Mydosh [21], it is possible to come to a conclusion: the three Co-rich compositions are in the same range as the metallic three-dimensional spin-glasses. The compound with the least Co ($x = 3$) has a significantly higher value and ends up closer to the insulating spin-glasses. This can also be understood, even though conductivity measurements have not been made, since the charge conducting medium (Co^{2-3+}) is gradually 'diluted', resulting in a decrease in conductivity. Here, it is possible to see the reason why the suggested T_f–C relations do not work for the present system: the $YBaCo_{4-x}Zn_xO_7$ system changes its conductivity with different x values in contrast to the previously studied metallic systems, where all the compared compounds had almost the same metallic properties, e.g., Mn_xCu_{1-x}.

4.1.3. Ac susceptibility—imaginary part. In the same way as for χ', there is an obvious scaling difference in the χ'' plots shown as functions of temperature (figure 4). The relative energy losses during the magnetic transition at T_f (χ''/χ') are 1.7, 1.1, 1.7 and 4.8% for $x = 0$–3, respectively. In all four compounds, the energy loss at the magnetic transition is significant, suggesting that the transitions themselves are non-spontaneous.

The maximum in χ'' (figure 4) appears just below the maximum of χ' (figure 3) and is also frequency-dependent, however the difference in temperature between the maxima changes significantly with the Co content. As an example, $T(\chi'_{\max}) - T(\chi''_{\max})$ values at 2125 Hz are: 0.21, 1.2, 0.71 and 0.40 K for $x = 0$–3, respectively. Why this difference changes irregularly is not understood.

In two of the compounds ($x = 0$ and 1), there is a second maximum or shoulder on the low-temperature side of $\chi''_{\max}$. Both these samples proved to be x-ray pure when examined with Guinier and diffractometer techniques [11, 12]. Hence, the samples must contain a second redistribution of magnetic spins, at ~10 K for $YBaCo_3ZnO_7$ and close to 45 K for $YBaCo_4O_7$. In trying to understand this, the amount of Co and the $T_f(\omega)$ relation of χ' has to be taken into consideration. At 45 K, there is a strong change in χ' for $YBaCo_4O_7$, however there is no obvious corresponding transition at 10 K for $YBaCo_3ZnO_7$. With an increase in Co content, the magnetic ions have more possibilities to couple. Hence, the reason for having two intensites in χ'' could mean either that (i) the frozen state distorts and again becomes partly liquified before the final frozen state occurs or (ii) there are two subsystems having two different freezing temperatures. Event (ii) is more likely since a frozen state is not likely to melt again during a lowering of temperature. If the first subsystem freezes at one point and has a typical frustrated nature, the overall magnetization is slightly anti-ferromagnetic,

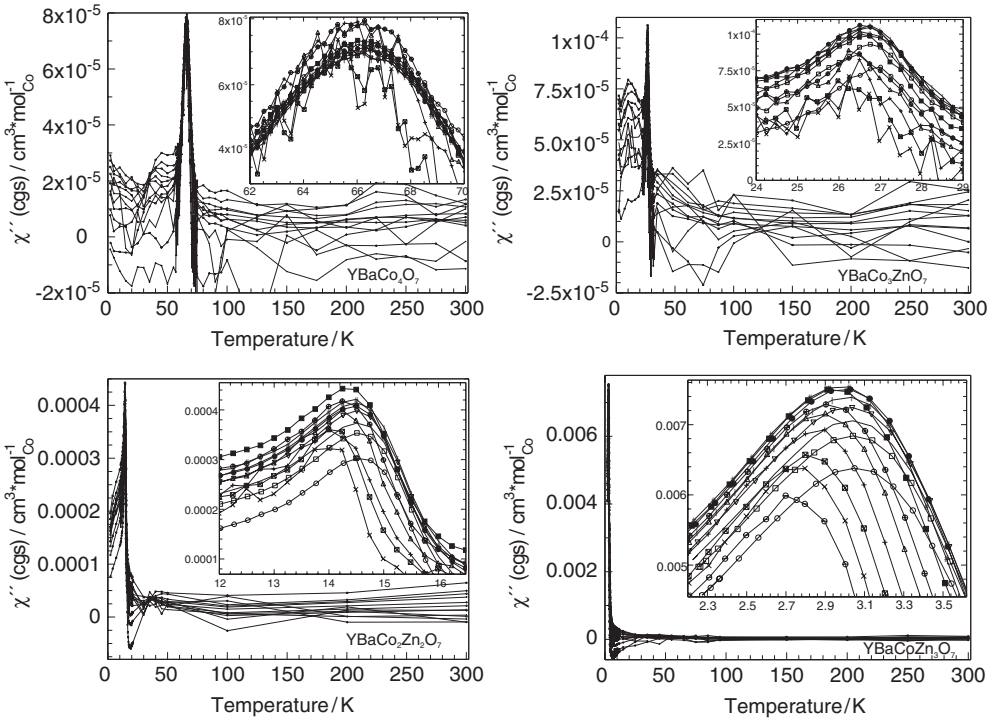

Figure 4. The imaginary magnetic susceptibility (χ''), using an ac field of 10 Oe, plotted versus temperature. The different compounds are indicated in the graphs and the inset is a magnification of the transition range. The measuring frequencies (in Hz) are: 75 (⊖), 125 (×), 225 (⊠), 425 (+), 825 (△), 1225 (⊕), 2125 (■), 3025 (#), 4025 (●), 5025 (|), 6025 (▽), 7025 (no marker), 8025 (□), 9975 (○).

since all four 'first' transitions act field repulsively. When the second system freezes, it starts competing with the already frozen anti-ferromagnetic state. This competetive second system is stronger in $YBaCo_4O_7$ than in $YBaCo_3ZnO_7$ and results in two different slopes of the $\chi'(T)$ curves below T_f. However, at ∼5 K, the second system, which contains more parallel spins (ferromagnetism), starts to dominate in strength, resulting in a final increase in χ'. Both of the 'second' transitions appear at ∼20 K below the 'first' transition, which explains why no second transition is seen for $YBaCo_2Zn_2O_7$ or $YBaCoZn_3O_7$.

There are no significant contributions in the real parts or the imaginary parts in the second and third harmonics of χ.

4.2. Magnetic calculations

By making a first Arrhenius plot it was possible, using extrapolation, to estimate T_0, which is called the ideal glass temperature. By placing this T_0 in the Vogel–Fulcher function [22] (figure 5(a)), displaying $\ln(\omega/\omega_0) = -E_a/(k_B \times (T_f - T_0))$, the activation energy (E_a) and the ground-state frequency (ω_0) were calculated [23]. Using again the ideal glass temperature from the Arrhenius calculations, the power law was applied to the data for extracting the dynamic exponents (zv) and more reasonable ω_0 frequencies (figure 5(b)). The whole procedure follows the guidelines given by Mydosh [21]. Results of the linear functions fitted to the experimental

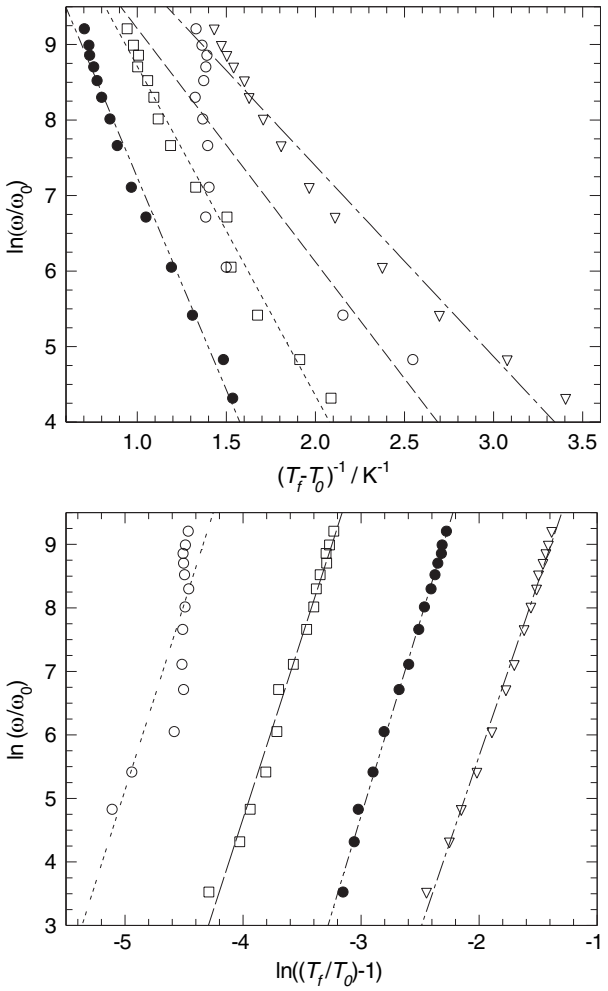

Figure 5. (a) The Vogel–Fulcher plot and (b) the power-law plot using the estimated T_f and the ac frequencies. The different compounds are marked as follows: $YBaCo_4O_7$ (○), $YBaCo_3ZnO_7$ (□), $YBaCo_2Zn_2O_7$ (●) and $YBaCoZn_3O_7$ (▽).

values are presented in table 1. Comparing the different curve fits using the Vogel–Fulcher or the power law, the latter seems to be a better method to model the variation in T_f by visually weighing the linear fit against the real data.

The T_0 values naturally end up on the low-temperature side of T_f and should equal that value of T_f as $\omega \to 0$. These results will be discussed when dc measurements are presented below. From the second fit, the Vogel–Fulcher, a reasonable value for the activation (E_a) of the melting process of the frozen magnetic state as well as a first approximation of the relaxation time can be extracted. All E_a values occur in the same range, meaning either that the crystal system is the deciding matter for the thermodynamic stability of the magnetic state or that the differences in energy are too small to be distinguished by this method. Also, the low E_a values mean that the energy levels are highly degenerate, which is a typical scenario for frustrated systems. Furthermore, these results are much more reasonble than those obtained with the Arrhenius approach (1000–3000 K). However, the relaxation times ($2\pi\omega_0{}^{-1}$) are also fairly

Table 1. The calculated values form the linear fittings in figures 5(a) and (b) and values for the saturation calculations.

	Equation						
	Arrhenius	Vogel–Fulcher: $y = -a \times x + b$			Power-law: $y = c \times x + d$		
Sample	T_0 (K)	$a(E_a)$ (K)	b	ω_0 (e^b) (Hz)	$c(zv)$	d	ω_0 (e^d) (Hz)
$YBaCo_4O_7$	65.67	3.09	12.3	2.20×10^5	5.9	34.4	8.7×10^{14}
$YBaCo_3ZnO_7$	26.79	4.36	13.1	4.89×10^5	5.7	27.6	9.7×10^{11}
$YBaCo_2Zn_2O_7$	13.89	5.63	12.9	4.00×10^5	6.1	23.1	1.3×10^{10}
$YBaCoZn_3O_7$	2.790	2.52	12.4	2.43×10^5	5.5	16.6	1.6×10^7

similar, which should not be, since the degree of frustration significantly changes between the compounds as described above with the large changes in Weiss constants. The power-law fit, which is the visually most accurate, gives totally different relaxation times, i.e., very short (10^{-14} s) to relatively long (10^{-7} s) throughout the series $x = 0$–3. $YBaCo_4O_7$ is examined further and compared with earlier results [11] where powder neutron diffraction was performed and a non-indexable magnetic contribution was detected. The fact that this contribution was present means that the magnetic structure has a relaxation time shorter than approximately 10^{-8} s. This relaxation time falls right inbetween the two calculated values for $YBaCo_4O_7$; 10^{-5} s (Vogel–Fulcher) and 10^{-14} s (power law). This means that the former relaxation time cannot be and that the latter is probable.

The dynamic exponent, zv, is fairly similar for all four compounds and in the range where spin-glasses are found.

With only four points, it is difficult to establish a relation, however an exponent t for the relation $T_f \propto C_{Co}^t$ [24] was calculated, where C_{Co} is the concentration of Co at the tetrahedral positions in the structure. From a least-squares fit, it is possible to extract $t \approx 2.1$, which is significantly larger than 0.63 for the Mn_xCu_{1-x} system [20]. This means that the change in Co content for the $YBaCo_{4-x}Zn_xO_7$ system has a relatively strong influence on T_f. If the system has an anisotropic magnetic property, it might not be correct to use this simple relation, since a more complex relation would be expected.

4.3. Magnetization

4.3.1. FC and ZFC. All four compounds exhibit differences between the FC and ZFC curves (figure 6). Only for the $YBaCo_4O_7$ compounds is it possible to see a complex behaviour in the transition temperature region, which depends on the fact that the $x = 0$ homologue has a relatively stable magnetic coupling and does not completely lose the 'anti-ferromagnetic' upturn as a result of an outer field of 0.1 T. The estimated transitions, where the direction of ZFC starts to deviate significantly from that of the FC curve, are about: 63, 27, 14 and 2.5 K for $x = 0$–3, respectively. These values are comparable with the T_0 from the ac measurements.

The fact that the difference between FC and ZFC curves already starts above T_f, as detected using an ac field, is previously observed in magnetic systems that slowly freeze over a large temperature range, e.g., spin-glasses (see, for example, [10]). Sharp transitions appear using a smaller field and the 0.1 T used in these measurements will hinder the flexibility of the spin-flopping already above T_f, although the field is far from saturating the material.

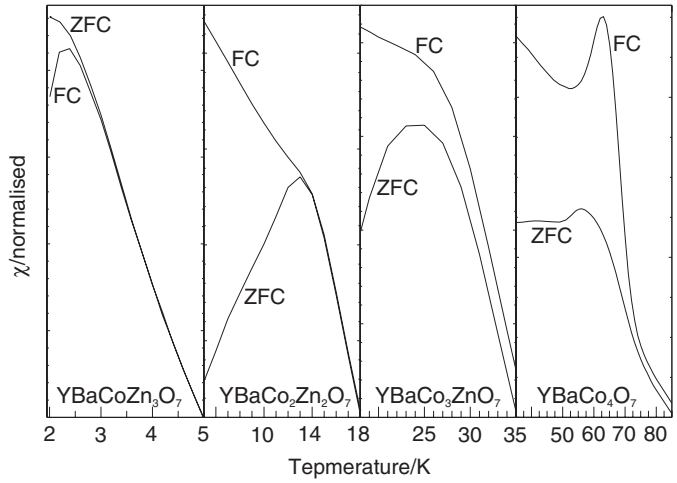

Figure 6. FC and ZFC measurements using 0.1 T as the cooling and measuring fields, respectively. χ is displayed as a function of temperature and normalized to increase the resolution over the transition range. The different stoichiometries are indicated below the curves.

As expected, FC results in a higher χ than ZFC data for three of the four compounds, but the $YBaCoZn_3O_7$ has the reversed relation, which is odd. One possibility is that a canted-anti-ferromagnetic-like situation, with a resulting magnetic moment, rules the ZFC frozen state. This canted state is partly cancelled or destroyed with the use of an outer field during the magnetic freezing process (FC), ending up in a more anti-ferromagnetic state.

4.3.2. Isothermic magnetization. The magnetic moment pro Co in figure 7 was calculated according to: Moment $= (4\pi/7) \times 10^{-4} \times$ emu $\times\, {n_{\mathrm{Co}}}^{-1}$, where n_{Co} is mol Co in the measured sample [18]. As expected, the moment is lower with higher Co content and its magnitude reveals that the interactions below T_f are chiefly anti-parallel, of which a part can be flipped by using the outer field. The saturation moment of Co is referred to as uncertain due to spin–orbit coupling, but in the case of $YBaCoZn_3O_7$ the moment almost reaches 1 μ_{B} at 8×10^4 Oe and 2 K; the other three compounds are far from saturation at 8×10^4 Oe, agreeing with a spin-glass-like state. All the magnetization measurements show the typical behaviour for paramagnetic materials at higher temperatures ($T \gg T_f$), i.e., the magnetization is proportional to the field. Closer to T_f, the relations are no longer proportional but exhibit parabolic behaviour that is stronger for the compounds with less Co, most likely due to the different magnetization magnitudes. Of these curves, it is possible to see that the linearity is broken at 85, 35, 20 and 10 K for $x = 0$–3, respectively, which in all cases is far above T_f. This suggests that some magnetic interaction energies become stronger than the thermal energy and that the transition already starts far above the T_f obtained from the ac measurements.

It is also obvious, especially for the compounds with more Co, that the curves reaching the highest magnetization are not at the lowest temperature. Instead, at the lowest temperature, the magnetic 'viscosity' seems to increase, resulting in relatively lower magnetization than found just below T_f.

All curves are smooth, having no abrupt increases in magnetization, meaning that all four compounds are without metamagnetic properties in fields up to 8 T.

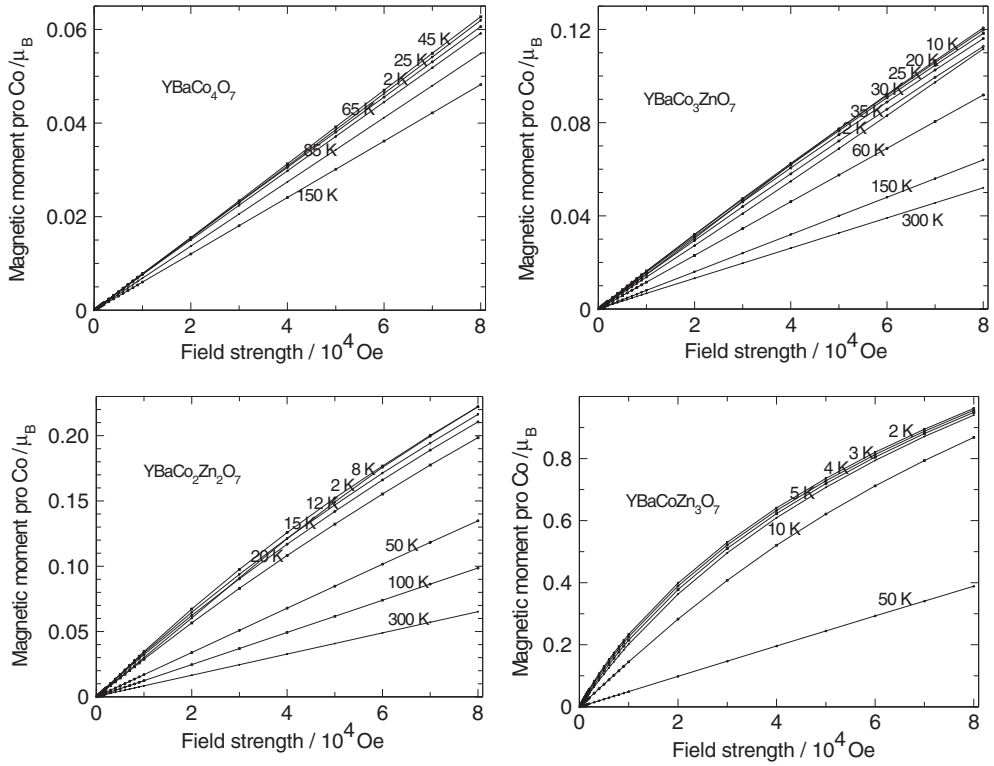

Figure 7. Magnetization displayed as a function of the applied magnetic field at temperatures indicated in the graphs. The lines are added to guide the eye.

4.3.3. Saturation fields of $YBaCo_4O_7$. The $YBaCo_4O_7$ was subject to further magnetization studies searching for new ways to use dc magnetization data, where the focus was on extracting a saturation field. The field dependency on field-cooling compared with the zero-field cooling was investigated (figure 8). Above the previously estimated T_f of 65 K, all χ versus T curves superimpose, which is what would be expected for a paramagnetic compound. Close to T_f, the curves start to split and the penetration of the external field increases almost proportionally to the field strength. When examined closely (figure 8, inset), χ increases in a more parabolic manner with increasing field, and functions of second order ($F(\chi) = gB_{\text{ext}}{}^2 + hB_{\text{ext}} + i$) could be fitted to the data with high accuracy. Using the fact that $\chi = B_{\text{int}}/B_{\text{ext}}$, the function can be transformed into $F(B_{\text{int}}) = gB_{\text{ext}}{}^3 + hB_{\text{ext}}{}^2 + iB_{\text{ext}}$. At a saturation point, the internal field does not change anymore, i.e., $F'(B_{\text{int}}) = 0$. Differentiation of the function gives $F'(B_{\text{int}}) = 3gB_{\text{ext}}{}^2 + 2hB_{\text{ext}} + i$. The normal procedure is used to find the two results for $F'(B_{\text{int}}) = 0$ ending up with the formula

$$B_{\text{ext}} = -\frac{h}{3g} \pm \sqrt{\left(\frac{h}{3g}\right)^2 - \left(\frac{i}{3g}\right)}.$$

All data for these calculations are presented in table 2 and values of B_{ext} are also set in graphical form (figure 9).

B_{ext} has one positive value, which will be used in further discussions. The negative value should be the field needed to compensate the magnetization reached in a ZFC sample. Note the values for 70 K represent 'paramagnetic' values since this is above T_f and the negative value

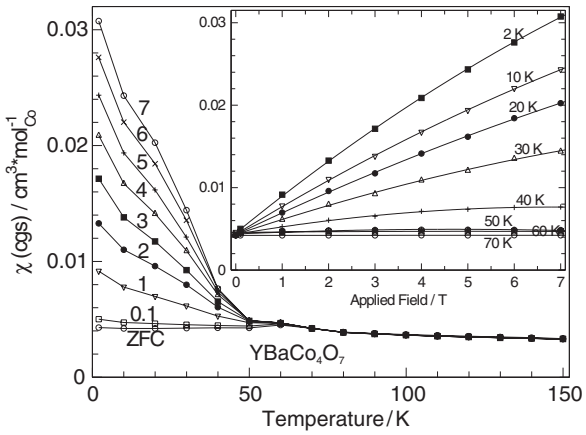

Figure 8. FC and ZFC dc magnetic measurements as functions of temperature. The field used for FC is indicated in the plot above the respective curve. The inset displays the resulting χ at several temperatures for the FC measurements. Second-order functions fitted to the curves according to $F(\chi) = gB_{\text{ext}}^2 + hB_{\text{ext}} + i$ (where B_{ext} is the applied field in tesla), have been refined to the curve and drawn as a solid line to the measured data points (markers). The values for g, h and i are presented in table 2.

is in the same order as the positive value, which is expected for a material without magnetic coupling. The values vary from one temperature to the next and the interpretation of this fact is that the magnetic properties in this material change nonlinearly with temperature. In fact, two different factors play an important role and could be set as variables in the function above according to: $B_{\text{ext}} =$ storability (SA) $\pm$ flexibility (FI). The most interesting value to compare is the ratio FI/SA, which will be called relative flexibility (RF).

The results from the calculations will now be discussed from high to low temperatures. Above T_f (70 K), SA is relatively small, but FI is high due to thermal movement and a field of about 50 T in either direction is needed to align all spins. Just below T_f, SA increases down to 50 K and RF decreases remarkably at the same time. At 40 K, there is a significant decrease in SA as well as a small increase in RF. This event coincides with the end of the second 'peak' in χ'' (figure 4) and a small decrease in χ' (figure 3), which was discussed above as a second redistribution of spins. This would explain the regional loss in SA and gain in RF. From 30 K down to 2 K, the SA as well as the RF stay fairly constant, justifying the idea that the magnetic structure is solidified. This new data analysis agrees with the above-presented ac data and increases the use of dc data, since a part of the magnetic flexibility is revealed as RF.

4.3.4. Magnetic relaxation. The magnetic relaxtion of $YBaCo_3ZnO_7$ (figure 10) is performed approximately 7 K below the observed T_f. This difference has to be chosen carefully to find the appropriate temperature for relaxing the thermoremanent magnetization [25]. For the examined compound, the different waiting times at 20 K did not result in any detectable ageing of the magnetic ordering, since the relaxations progress similarly for all waiting times, meaning that the magnetic properties of $YBaCo_3ZnO_7$ are not due to site-disorder effects. One important feature can be observed; the relaxation passes zero, entering into the negative half of the magnetization range. Note that the 30 s measurement has the smallest negative turn before the final relaxation, while the 9000 s data have the largest negative dip at $\sim$2500 s of relaxation. The reason for this event could be that the compound has an initial induced ferromagnetic order but contains, before complete relaxation, a subsequent second state with

Table 2. Refined and calculated values for the magnetization curves belonging to $YBaCo_4O_7$.

	Temperature (K)							
	2	10	20	30	40	50	60	70[a]
g	-1.22×10^{-4}	-8.36×10^{-5}	-5.79×10^{-5}	-6.3×10^{-5}	-7.14×10^{-5}	-2.62×10^{-5}	-5.38×10^{-6}	-5.38×10^{-7}
h	4.6×10^{-3}	3.44×10^{-3}	2.68×10^{-3}	1.89×10^{-3}	9.71×10^{-4}	2.45×10^{-4}	5.36×10^{-5}	4.76×10^{-7}
i	4.5×10^{-3}	4.34×10^{-3}	4.32×10^{-3}	4.31×10^{-3}	4.34×10^{-3}	4.38×10^{-3}	4.57×10^{-3}	4.21×10^{-3}
SA	12.6	13.7	15.4	10.0	4.53	31.2	3.32	0.295
FI	13.0	14.3	16.2	11.1	6.39	32.1	17.2	51.1
RF	1.03	1.04	1.05	1.11	1.41	1.03	5.18	173

[a] Above T_f.

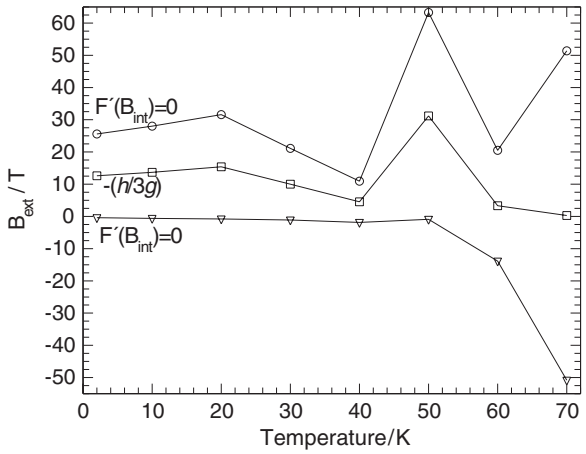

Figure 9. Graphic form of the results from table 2. □, SA; ○, SA+FI; △, SA-FI. The latter two are the limits where saturations are reached; $F'(B_{\rm int}) = 0$.

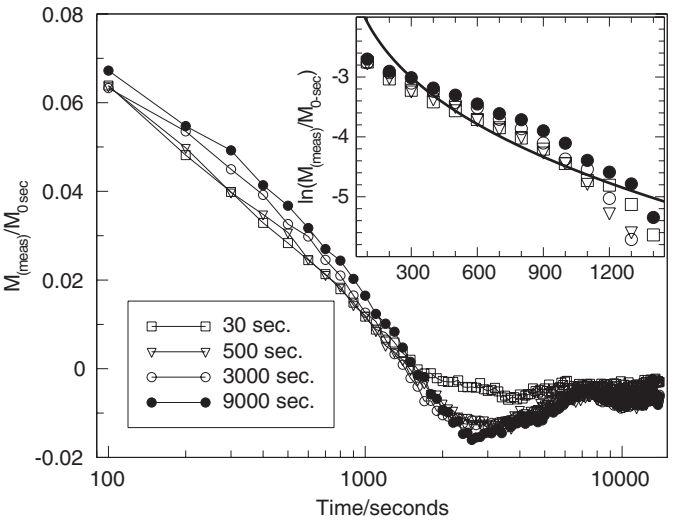

Figure 10. The thermoremanent magnetization for $YBaCo_3ZnO_7$ plotted as a function of time. $M_{0\,\rm sec}$ is the first measurement made before the applied field was shut off (at zero time). M_T is the magnetization in the sample at the time indicated on the x-axis. The different waiting times at 20 K are indicated with different symbols according to the inset (lower left). Measuring procedure: start at 50 K—0.1 T applied—cool to 20 K—waiting time (indicated in the inset)—$M_{0\,\rm sec}$ measured—field off—start measurements, time is zero. The inset (upper right) is the same data over a smaller temperature region. Added as a line is the function $Y = \alpha\tau^{(1/3)}$, where $\alpha = -0.45$, Y is $\ln(M_{\rm meas}/M_{0\,\rm sec})$, and τ is the time.

dominantly anti-parallel magnetic interactions that relax during a relatively longer time. If we assume that the induced magnetism only relaxes and has no re-entry effects, it is possible to give an interpretation; the system contains two relaxing magnetic subsystems, of which the stronger one contains anti-parallel interactions. The second, weaker system is of unknown type but weak enough to stay parallel to the outer field during the cooling through T_f. The outer

field induces the weaker subsystem with parallel spins but also causes the stronger subsystem to freeze as more anti-parallel, i.e., the weaker system stabilizes the stronger. When the outer field is shut off, the weak (ferro-) system relaxes relatively quickly in about 2500 s, but leaves an unstable stronger subsystem behind. As a second event, the now unstabilized (anti-ferro-) system relaxes for 4500 s (up to ∼7000 s). Naturally, the stronger system might relax during the whole time range, but its change is too small to be detected before the weaker system has relaxed. The reason for the smaller dip at 2500 s with the 30 s data is probably because the weaker system, which results as soon as the ageing is initiated, starts to stabilize the stronger system but the time is too short for the stronger system to evolve; with longer waiting times the stronger subsystem is developed. Thus, the 9000 s data contain the largest 'anti-ferromagnetic' dip in comparison with the other three measurements.

In the inset to figure 10, a logarithmic fit has been added to see how the present system relaxes in comparison with a model system. The exponent $(1 - n)$ in the formula $M(\tau) = M(0)\exp(\alpha \times \tau^{(1-n)})$, in which τ is the time, has the model value $1/3$ for spin-glasses [9]. This value gives a relatively good fit for the time span 300–1300 s. The α value is refined with least-square refinement to -0.45. The problem arising for this system is that the values of $M_{\mathrm{meas}}/M_{0\,\mathrm{sec}}$ become negative later than 1000 s.

5. Conclusion

When replacing Co with Zn, the properties of the material change similarly to the dilution effect for systems where the percolation limit is examined. However, in this system, the atomic positions of the magnetic inclusion are not random, as in the Mn_xCu_{1-x} alloy [20], but instead more similar to the spinel $CdCr_{2x}In_{2-2x}S_4$ [26] and the plumbite $SrCr_{9p}Ga_{12-9p}O_{19}$ [27] systems, where the magnetic ions (Cr^{3+}) are randomly distributed at special positions in the structure. The spinel is highly symmetric and should have no anisotropic properties, but the plumbite has, just like the title compounds, a hexagonal symmetry and develops several possibilities for anisotropy. If the properties result from two underlying magnetic subsystems developed in two crystallographic directions, different properties might be observed depending on the 'concentration' of the magnetic ion. The two above-mentioned Cr systems also have more than one crystallographic position for the magnetic ion, however the system presented here seems to develop high anisotropy and thus two possible magnetic subsystems that are competing; the stronger one has a more anti-ferromagnetic character while the weaker one a more ferromagnetic character. Two competing magnetic effects have also caused spin-glass properties to appear in the system $Eu_{1-x}Gd_xS$ [28].

Apart from this fact, there are two reorderings of spins seen in the χ'' (figure 4) and there is a re-entry of parallel interactions with higher Co content below 5 K in χ' (figure 3) with high Co content. Also, there should be at least two relaxing magnetic entities, since the relaxation measurements enter negative values after relaxing the weak, 'ferromagnetic' substructure, leaving the stronger 'anti-ferromagnetic' substructure to relax during a larger time-window.

Using the data from the structural investigations of $YBaCo_4O_7$ [11], it is possible to calculate the different Co–O–Co bond angles at three different temperatures (figure 11). At lower temperatures, the apical bonds (along z) are closer to 90°, which would make the interactions along the unique axis stronger than those in the plane, assuming that super-exchange applies [29].

The fact that Co in the structure prefers the 2*a* position (Co1) helps explain the magnetic properties: at low Co content ($x = 2$ and 3), the apical interactions are almost the only ones present and they are dominantly anti-parallel, since all $\chi(T)$ data point to this. When enough

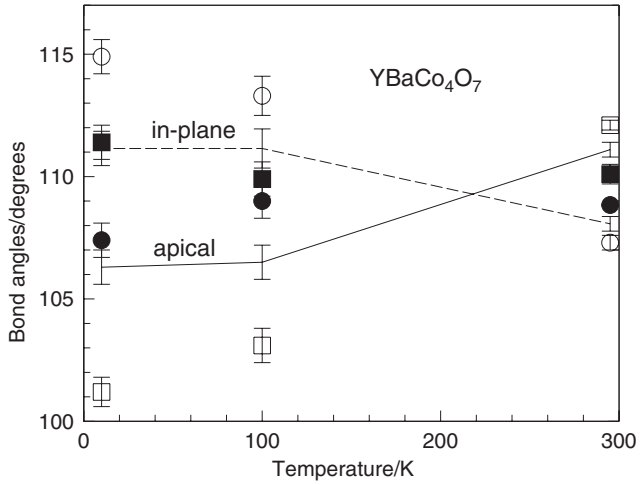

Figure 11. The Co–O–Co angles plotted versus temperature for $YBaCo_4O_7$ ($x = 0$) [11]. The different angles are presented as follows: Co2–O2–Co2 (●), Co2–O1–Co2 (○), Co1–O2–Co2 (■) and Co1–O3–Co2 (□). The solid line represents the average of the apical bonds (■□) and the broken line represents the average in-plane bonds (●○). All data are plotted with standard error bars.

Co is present ($x = 1$), the in-plane interactions, assumed here to be more parallel, start to compete with the axial interactions. Therefore, χ does not decrease below T_f to the same degree as for $x = 2$ and 3. This effect is even more developed for the compound with only Co ($x = 0$), where χ flattens out 5–10° below T_f. It seems that the parallel interactions (in-plane) get stronger with a decrease in temperature, since a ferromagnetic increase in χ appears for the $x = 0$ and 1 compounds over the range 5–10 K, as already mentioned above. Using the assumptions that in-plane interactions are more 'ferro-' and occur below T_f, and that the apical 'anti-ferro-' interactions are the events dominating at T_f helps to explain the situation; the relaxation measurements show a fast relaxing 'ferromagnetic' feature and a lasting 'anti-ferromagnetic' interaction because the measuring temperature was in the range between the two magnetic reordering temperatures according to the χ'' results (27 and ~10 K). Hence, the in-plane (ferro-) interactions had not evolved enough in comparison with the axial (anti-ferro-) interactions at 20 K in $YBaCo_3ZnO_7$.

Discussing the percolation limit, Co has six possibilities to get involved in super-exchange interactions (figure 1), which would set a theoretical percolation limit of 1/6 Co at the tetrahedral sites if only short range order is needed to create the magnetic interactions. However, the two different sites (Co1-2*a* and Co2-6*c*) have different environments, i.e., 2*a* can only couple to six 6*c* sites, but 6*c* has two options: two interactions with 2*a* and four with itself (6*c*). Hence, if only Co was placed at 2*a*, the percolation limit would be 1/4, since all 6*c* positions would contain Zn. The same limit is valid for the reverse event; Co is only found at the 6*c* site. Through this logic, it is possible to understand that the mixed occupancy is an advantageous situation, since the theoretical percolation limit becomes smaller (1/6).

The system presented here contains almost the same property with 25–100% Co at the tetrahedral sites, in contrast to several other systems where different magnetic properties appear at different concentrations of magnetic ions, e.g., $La_{2-x}Sr_xCuO_4$ (spin-glass to superconductivity) [9], $CdCr_{2x}In_{2-2x}S_4$ (spin-glass to ferromagnetism) [26] and $Fe_xZn_{1-x}F_2$ (spin-glass to anti-ferromagnetism) [30]. The persistent disordered magnetic properties of $YBaCo_{4-x}Zn_xO_7$ ($x = 0$–3) must therefore be a result of extreme frustration.

Due to the complex magnetic nature of the presented compounds, they cannot be placed in a yet known property class. The frequency-dependent T_f, the calculated dynamic exponents ($z\nu$), and the onset of χ'' just below χ' are typical evidences for a spin-glass. At the same time, the broadness of the transition in the dc measurements (figure 7) and the full relaxation (figure 10) are not indications of spin-glasses but rather of a superparamagnet. The common net of tetrahedra in the structure contains a 3D geometrical frustration and could contain charge disorder (Co^{2+}, Co^{3+}) and substitutional disorder (Co/Zn), as well.

Most probably, the compounds presented here contain a spin-glass feature together with a second magnetic type, of which a disordered anti-ferromagnet or a cluster formation (superparamagnetism) is possible. However, the magnetic properties in the series $YBaCo_{4-x}Zn_xO_7$ as a whole should be described as changing from disordered anti-ferromagnets to spin-glasses as x increases.

Acknowledgments

I would like to thank the Foundation Blanceflor Boncompagni-Ludovisi née Bildt and the Alexander von Humboldt Foundation for endorsing this project with research grants. I am also grateful to Dr Manfred Möller and Dr Rolf-Dieter Hoffmann for assistance in performing the magnetization measurements. Professor Rainer Pöttgen is acknowledged for his hospitality, allowing me to stay in his group during the final stages of this work. Furthermore, many thanks go to Professor J A Mydosh for interesting and constructive comments.

References

[1] Reimers J N, Greedan J E, Kremer R K, Gmelin E and Subramanian M A 1991 *Phys. Rev.* B **43** 3387
[2] Reimers J N, Greedan J E, Stager C V, Bjorgvinnsen M and Subramanian M A 1991 *Phys. Rev.* B **43** 5692
[3] Gaulin B D, Reimers J N, Mason T E, Greedan J E and Tun Z 1992 *Phys. Rev. Lett.* **69** 3244
[4] Gingras M J P, Stager C V, Raju N P, Gaulin B D and Greedan J E 1997 *Phys. Rev. Lett.* **78** 947
[5] Jana Y M, Sakai O, Higashinaka R, Fukazawa H, Maeno Y, Dasgupta P and Ghosh D 2003 *Phys. Rev.* B **68** 174413
[6] Muraoka Y, Tabata H and Kawai T 2000 *J. Appl. Phys.* **88** 7223
[7] Petrakovskii G A, Aleksandrov K S, Bezmaternikh L N, Aplesnin S S, Roessli B, Semadeni F, Amato A, Baines C, Bartolomé J and Evangelisti M 2000 *Preprint* cond-mat/0011055v1
[8] Matsuno K *et al* 2003 *Phys. Rev. Lett.* **90** 096404
[9] Wakimoto S, Ueki S, Endoh Y and Yamada K 2000 *Phys. Rev.* B **62** 3547
[10] Cardoso C A, Araujo-Moreira F M, Awana V P S, Takayama-Muromachi E, de Lima O F, Yamauchi H and Karppinen M 2003 *Phys. Rev.* B **67** 020407 (R)
[11] Valldor M and Andersson M 2002 *Solid State Sci.* **4** 923
[12] Valldor M 2004 *Solid State Sci.* **6** 251
[13] Müller-Buschbaum H and Rabbow C 1996 *Z. Naturforsch.* B **51** 343
[14] Müller-Buschbaum H, Rabbow C and Panzer S 1997 *Z. Naturforsch.* B **52** 546
[15] Redman M J and Steward E G 1962 *Nature* **193** 867
[16] Ritchey I, Chandra P and Coleman P 1993 *Phys. Rev.* B **47** 15342
[17] Kosterlitz J M and Thouless D J 1973 *J. Phys.: Condens. Matter* **6** 1181
[18] Weiss A and Witte H 1982 *Magnetochemie* (Weinheim: Verlag Chemie)
[19] Tholence J L 1979 *J. Appl. Phys.* **50** 7310
[20] Mulder C A M, van Duyneveldt A J and Mydosh J A 1981 *Phys. Rev.* B **23** 1384
[21] Mydosh J A 1993 *Spin Glasses: An Experimental Introduction* (London: Taylor and Francis)
[22] Vogel H 1921 *Phys. Z.* **22** 645
Fulcher G S 1925 *J. Am. Ceram. Soc.* **8** 339
[23] Tholence J L 1980 *Solid State Commun.* **35** 113
[24] Cannella V 1973 *Amorphous Magnetism* (New York: Plenum) p 195
[25] Wills A S, Dupuis V, Vincent E, Hammann J and Calemczuk R 2000 *Phys. Rev.* B **62** R9264

[26] Viticoli S, Fiorani D, Nogués M and Dormann J L 1982 *Phys. Rev.* B **26** 6085
[27] Obradors X, Labarta A, Isalgue A, Tejada J, Rodriguez J and Pernet M 1988 *Solid State Commun.* **65** 189
[28] Tholence J L, Holtzberg F, McGuire T R, von Molnar S and Tournier R 1979 *J. Appl. Phys.* **50** 7350
[29] Anderson P W 1959 *Phys. Rev.* **115** 2
[30] Belanger D P, Murray Wm E Jr, Montenegro F C, King A R, Jaccarino V and Erwin R W 1991 *Phys. Rev.* B **44** 2161